Oxygen Production by Electrolysis of Molten Lunar Regolith

L. A. Haskin
Department of Earth and Planetary Sciences
Washington University

Introduction

Previous work has shown that FeO and O_2 can be derived by electrolysis from silicate melt of a composition typical of lunar soils (Oppenheim 1968, Lindstrom and Haskin 1979). In the present study, we attempt to further refine the conditions necessary to optimize production and to determine efficiencies of production (how much product is derived for a given current) and purity of products.

Our goal in this study has been threefold. First, we want to define the theoretical energy requirements of the process. This includes studies of the relevant oxidation-reduction reactions in the melt, their kinetics and energies of reaction, and experimental determination of production efficiencies and melt resistivities as functions of melt composition and applied potential.

Second, we want to characterize the product(s) of silicate electrolysis. This includes evaluating the phase relationships in the systems SiO_2-TiO_2-Al_2O_3-MgO-FeO-CaO and Fe-Si; estimating the compositions of the metal products as a function of applied potential and feedstock composition based on phase equilibria in the Fe-Si system and free energy values for SiO_2 and FeO reported in the literature; definition of compositions of products in actual experiments; and definition of the form the product takes, whether phases separate or remain fixed, whether crystals settle or float in the remaining melt, and how large crystals form.

Third, we want to identify materials that can serve as electrodes and container materials for these highly corrosive high-temperature silicate melts. This includes identifying materials that may be either inert or thermodynamically stable in these melts, and experimental testing of the materials to confirm that they do not deteriorate. The ensuing report discusses our results within this framework.

Theory

We now understand in some detail the chemistry of the oxidation-reduction reactions involved in the electrolysis of silicate melts. This includes identifying the reactions involved and studying their kinetics, evaluating the dependence of oxygen production efficiency on melt composition, and determining the resistivities of melts as a function of composition. Much of this work is currently in final revision before publication (Haskin et al. 1990).

We have identified the cathode reactions that produce melt as the following:

$$Fe^{2+} + 2e^- = Fe^o \quad (1)$$

$$Si(IV) + 4e^- = Si^o \; . \quad (2)$$

Based on comparison with reductions of other cations such as Ni, Co, and Zn, these reactions are fast and will present no kinetics problems at current-densities needed to produce oxygen at a sufficiently high rate. Competing reactions at the cathode include the reductions of trace and minor melts, such as Cr, Ti, Mn, and Ni, and the reduction of oxygen dissolved in the silicate melt.

At the anode, the principal reaction is

$$4(SiO^-) = 2(Si\text{-}O\text{-}Si) + O^{2-} + 4e^- \; . \quad (3)$$

The kinetics of this reaction are also fast.

A serious competing reaction at the anode in melts with high iron concentrations is oxidation of Fe^{2+}

$$Fe^{2+} = Fe^{3+} + e^- \; . \quad (4)$$

Other competing reactions at the anode include oxidation of other multivalent cations such as Ti and Cr.

We identify the variables important in calculating the energy required by the electrolysis process as follows: Power to drive the electrolysis equals E*I, where I is the current required to get oxygen at the desired rate and is proportional to oxygen production rate/oxygen production efficiency. This demonstrates the dependence of power requirements on oxygen production efficiency. E is the potential required to drive the electrolysis and is equal to $E_c - E_a - \eta_c - \eta_a - I(R_{cell})$, where $E_c - E_a$ is the potential required to drive the reaction(s) and is a function of the cation reduced ($|E_c - E_a|$ increases in the order Fe < Si,Ti < Mg,Al < Ca) and the concentrations of the cations in the melt. The quantity $-\eta_c - \eta_a$ is the overpotential required because of slow reaction kinetics or, as we use it in this paper, because of cation mobility problems (inability of cations to migrate to the cathode fast enough to yield the desired production rate). R_{cell} is the resistance of the electrolysis cell and is equal to $L/\kappa A$, where L is the distance between electrodes, A is the electrode surfac area, and κ is the melt conductivity. This expression illustrates the dependence of power on both cell configuration and resistivity of the molten feedstock. Not unexpectedly, κ is found to increase as the average ionic mobility of the melt increases. That is, κ increases systematically as mobile cations such as Fe, Mg, and Ca increase relative to Si and Al in the melt.

We have now determined values for most of the variables identified in the discussion above. Because reaction (4) is the primary competing reaction at the anode, the efficiency of oxygen production (defined as moles O_2 produced/4 moles electrons passed through the melt) depends primarily on the concentration of Fe^{2+} cations. The dependence of oxygen production efficiency on Fe^{2+} concentration can be expressed as $\%O_2/(100 - \%O_2) \cong 0.049/X_{FeO}$, where $\%O_2$ is the oxygen production efficiency as a percentage and X_{FeO} is molar fraction FeO in the melt (see Figure 1.21). This has the consequence that electrolysis to produce oxygen as a main product is most efficiently carried out in melts with relatively low iron concentrations (<2%).

We have reported conductivities of molten silicates with compositions similar to those of molten lunar rocks and soils in the temperature range 1420-1550° (Haskin et al. 1990). The values lie in the range 0.08–40 $ohms^{-1}\,cm^{-1}$. These values appear adequate for robust cell design. A systematic variation in conductivity with composition is observed. The theoretically expected variation of conductivity with composition at

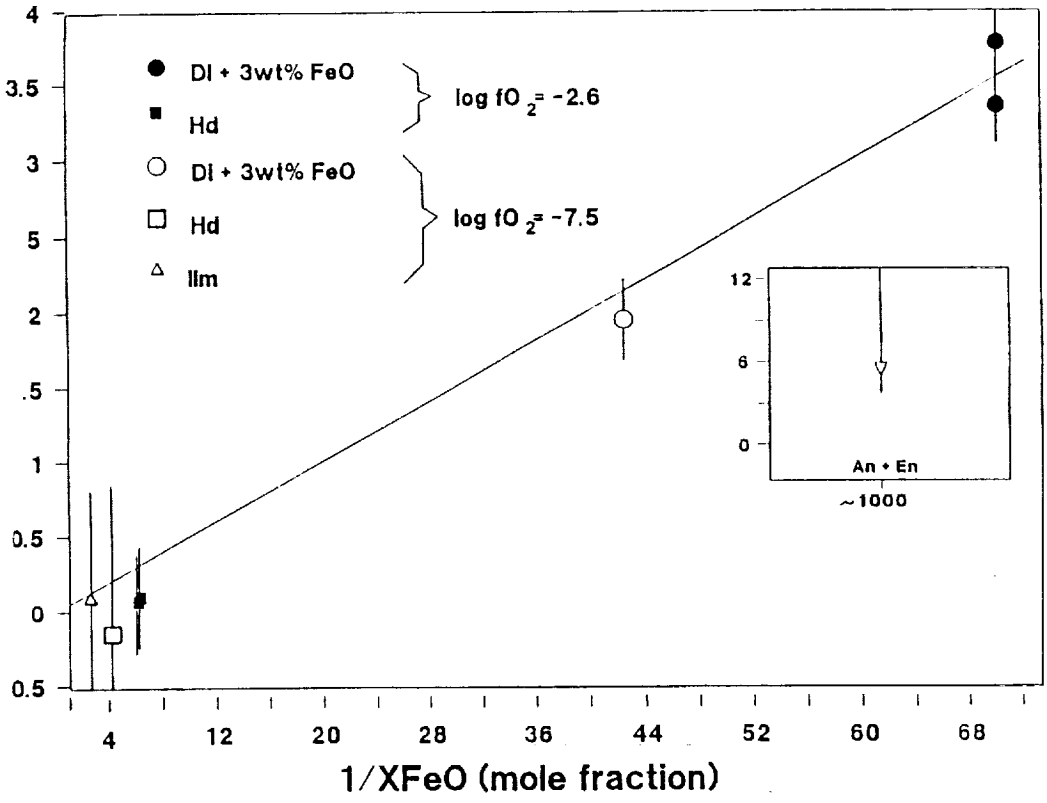

Figure 1.21 Diagram from Haskin et al. (1990) showing the dependence of oxygen production efficiency (defined in text) on concentration of ferrous iron in the melt.

constant temperature can be expressed by

$$\text{Conductivity} \propto \Sigma X_i D_i Z_i^2 ,$$

where X_i is the molar concentration of i, D_i is diffusivity of i, and Z_i is the charge of i (Reiger 1987, p. 160). This expression is similar to the relationship we observe between composition and conductivity, permitting conductivity to be predicted for any given composition.

We have found no kinetic problems associated with either anodic or cathodic reactions (both reactions being fast at the expected current-densities) and therefore expect low overpotentials arising from kinetic problems. We are now studying dynamic problems in the electrolysis and how they relate to overpotentials needed to drive reductions in the melt. We are studying whether material flow and thermal convection in a cell can keep fresh material at the electrodes or whether active mixing will be necessary.

New experiments are currently underway that will extend some of these results to compositions more typical of lunar soils. These experiments include a study of redox reactions for various cations in silicate melts of basaltic composition (similar to Apollo 12 soil) and compositions along the join Diopside ($Mg_2Si_2O_6$)-Anorthite ($CaAl_2Si_2O_8$). These studies will demonstrate how the potential required to reduce various species changes as a function of composition [extending the results of Semkow and Haskin (1985) to more realtistic soil compositions], as well as confirm that there are no kinetic problems with the reactions in these more realistic melts. Figure 1.22 shows preliminary results of these experiments illustrating the shift in Ni reduction potential as a function of silicate melt polymerization.

Characterization of Products

Based on known phase equilibria in basaltic systems; on phase equilibria in the system Fe-Si; on thermodynamic data for the reduction of the cations of Fe, Si, Al, Ti, Mg, and Ca; and on our experiments already reported (Lindstrom and Haskin 1979, Semkow and Haskin 1985, Colson and Haskin 1990a,b), we expect the products of silicate electrolysis to be as follows (at a temperature of, for example, 1350°C and at a reduction potential of about -1.5 volts):

> *Predictions From Theory*: Two or three metal phases form at the cathode (depending on the Si/Fe ratio of the bulk metal). These metal phases will contain varying amounts of Si, Fe, Cr, Mn, and Ti (and small amounts of trace constituents such as Ni), with the Si/Fe ratio of each phase

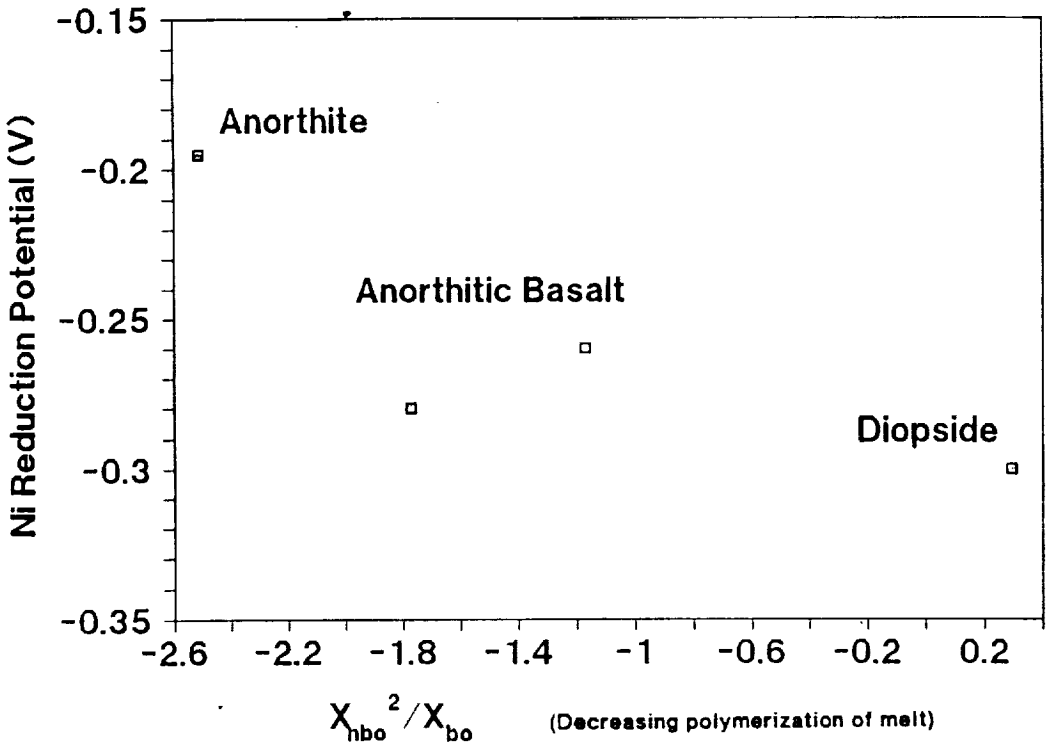

Figure 1.22 Diagram showing the dependence of Ni reduction potential on polymerization of the melt. X_{nbo} and X_{bo} are fraction non-bridging (Si-O) and bridging (Si-O-Si) oxygens, respectively. Trend is opposite of that expected and that reported by Semkow and Haskin (1985).

roughly defined by the Si-Fe phase diagram. Oxygen is liberated at the anode. Depending on the temperature and extent of SiO_2 removal, spinel $(Mg,Fe)(Al,Cr)_2O_4$ is expected to precipitate from the residual melt.

We have now begun a new set of experiments designed to test these predictions. These experiments are designed so that current and cell resistance can be measured and potential controlled simultaneously. This permits results to be interpreted in light of a known value for E_c - E_a. All measurements are made and instruments controlled by an AT-type personal computer attached to the instruments by an IEEE-488 bus. A diagram of the experimental circuitry is shown in Figure 1.23.

Results of these experiments should define product compositions as a function of feedstock, applied potential, and extent of electrolysis, thereby testing theory. They should give a qualitative idea of how cell resistance changes with extent of electrolysis, again testing theory. They should give a semi-quantitative estimate of the overpotentials required to drive the electrolysis and how the required overpotentials

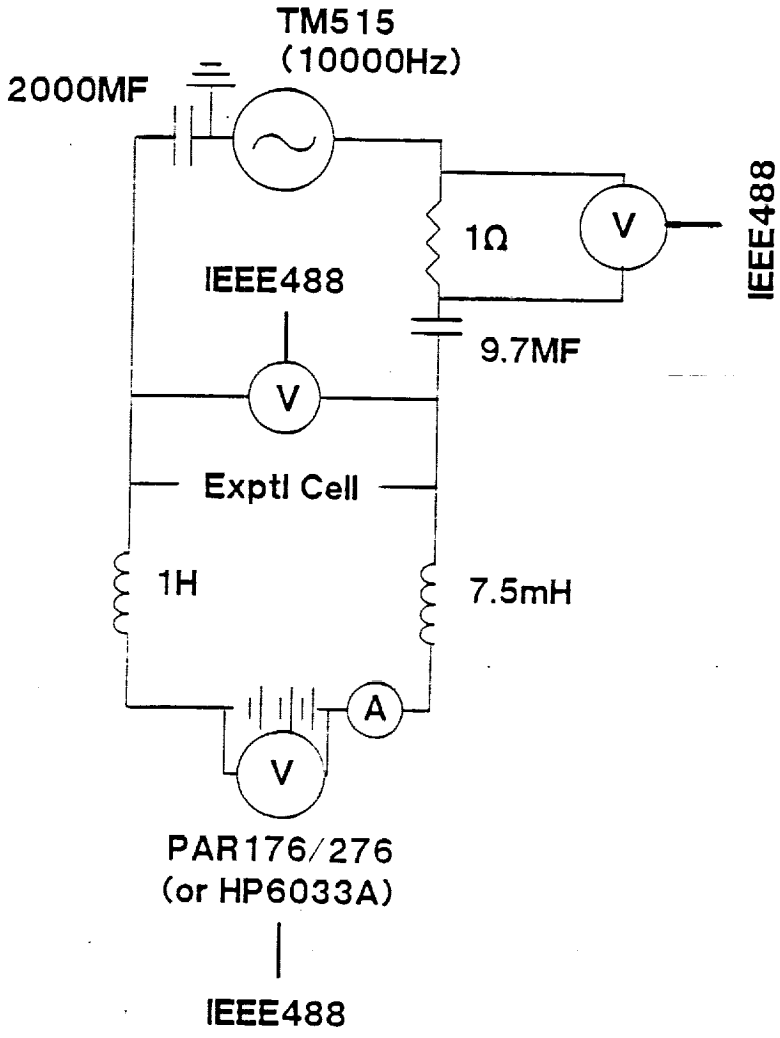

Figure 1.23 Diagram of circuit designed to measure cell resistance (via the 10000-Hz waveform generator and voltmeters) and control the DC potential (via the PAR 176/276 for current <1A, or the HP6033A for higher currents). IEEE-488 bus lines go to an AT-type computer that controls the experiment.

affect product composition. They should define the behavior of the products, whether the products float or sink, whether they separate or mix with other products, and what size of crystals or crystal aggregates are formed. As discussed below, these experiments also give a handle on the durability of the chosen electrode materials.

Preliminary experiments (each sample about 80 mg, mounted on a small Pt wire loop with temperature, atmosphere, and electrode potential controlled) show that the phase equilibria and metal phase compositions vary in a manner similar to that predicted from theoretical calculations, with Si/Fe ratio in the product melt increasing

with increasing potential and spinel crystallizing as SiO_2 removed from the melt (at 1350°C). The metal has a somewhat lower Si/Fe ratio than expected, possibly reflecting the lower mobility of Si in the melt relative to Fe.

Microprobe analyses of products from two experiments are reported in Table 1.8, illustrating the effects of applied potential and initial magma composition on metal composition, oxygen production efficiency, and spinel composition. The difference in composition between the two is that the second is like the first, with Si and Fe removed in the proportions expected to be removed by the electrolysis. Therefore, to some degree, these two illustrate how compositions change with extent of electrolysis.

Experiment A12_1, an electrolysis of an Apollo 12-soil-like composition, contains Fe-Cr-rich spinel and nearly pure Fe metal, and has a low oxygen production efficiency (28%). Experiment A12_1cb, which was at a higher potential with lower Si and Fe in the initial melt, contains Mg-Al-rich spinel, three distinct Fe-Si phases that contain significant amounts of Ti and Cr (the presence of Ir is due to use of Ir as the cathode material in these experiments), and somewhat higher oxygen production efficiency (45%). A backscattered electron image of the three metal phases is shown in Figure 1.24.

Testing of Electrode and Container Materials

We have suggested that Si may make a suitable cathode material (Haskin et al. 1990). We have made several efforts to test Si experimentally, but have run into difficulty mounting the Si as a cathode in our experiments. The Si cannot be mounted to Pt because of the low Si-Pt eutectic. We have tried welding the Si to Ir but, so far, the Si has either broken away from the weld-joint or has reacted with C in the reducing acetylene flame. We have tried mounting the Si to tungsten, but the tungsten oxidizes under our experimental conditions.

We have suggested the use of Pt as anode material (Haskin et al. 1990). There are also some experimental difficulties with testing the Pt as an anode, linked primarily to the small scale of our experiments. Even if the Pt lost from the anode was 10% of the amount of oxygen generated, it would not necessarily be apparent from looking at the electrode after the experiment that any Pt was lost, because the total Pt mass is large compared to the mass of oxygen generated. However, we have taken an alternative approach to estimating the Pt lost from the anode. We note that any Pt lost would be dissolved in the silicate melt and ultimately reduced to metal at the cathode. We have analyzed for Pt in the silicate glass and metal product of our electrolysis experiments (by electron microprobe) and have detected a Pt peak (Figure 1.25), suggesting that

Table 1.8 Microprobe analyses of metals and glasses in two experiments in Apollo 12-like melts.[a]

a. Metal Phase(s).

	A12_1		A12_1cb	
Si	0.024	2.471	6.999	7.389
Ti	0.040	0.142	0.464	0.581
Cr	-0.007	0.567	0.370	0.356
Mn	-0.037	0.231	0.041	0.037
Fe	92.13	33.12	29.28	30.06
Ir	0.000	56.40	56.50	56.40
Pt	-0.021	--	--	--

b. Glass and Spinel+Glass (S+G).

	A12_1		A12_1cb	
	Glass	S+G	Glass	S+G
SiO_2	49.48	0.13	49.21	48.07
TiO_2	2.34	1.16	2.76	2.78
Al_2O_3	10.78	9.10	18.92	19.31
FeO	13.23	42.37	0.69	0.41
MgO	10.09	12.63	14.23	14.69
CaO	9.96	0.31	12.48	11.99
Na_2O	1.12	-0.01	0.82	0.70
K_2O	0.10	0.00	0.08	0.08

[a] A12_1cb has lower initial Fe and Si and a higher applied potential than A12_1. Metal in A12_1 is nearly pure Fe (the low totals <100% is likely due to oxidation of the Fe during quenching of the experiment). Metal in A12_1cb contains significant Si, Ti, Cr, and possibly Mn. The presence of Ir in metals of A12_1cb is due to use of Ir as the cathode material. Otherwise, the compositions correspond to the phases γ-Fe, α-Fe, and melt in the system Fe-Si. Spinel grains were too small to analyze and, therefore, the analyses of spinel include glass as well. In the case of A12_1cb, the glass constitues the major portion of the analysis. Spinel in A12_1 is Fe-Cr rich; spinel in A12_1cb is apparently Mg-Al rich.

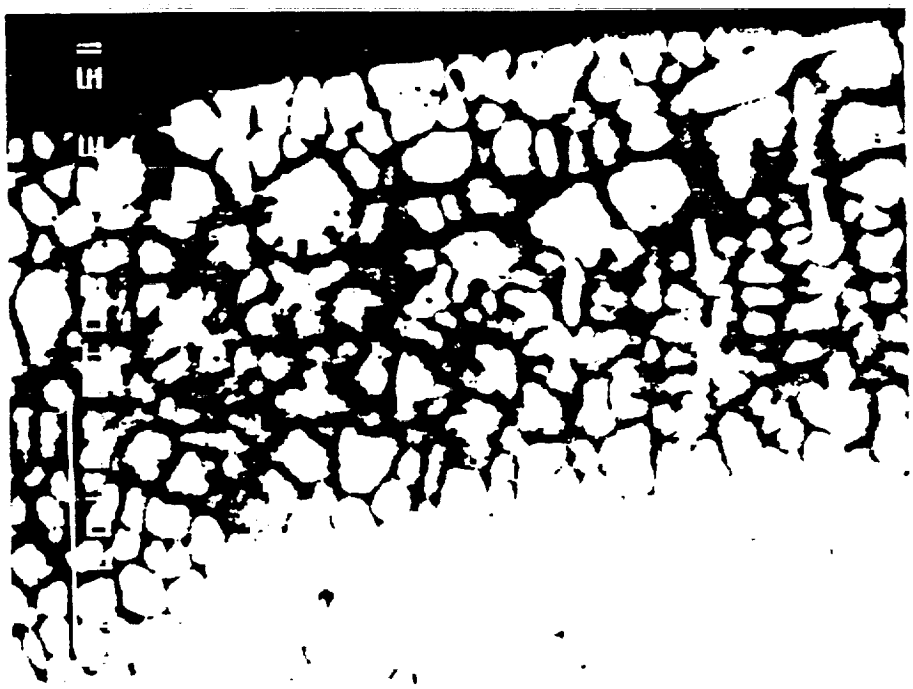

Figure 1.24 Backscattered electron image of the three metal phases in A12_1cb showing differences in density (white is more iron-rich, black is more Si-rich) and the mixed nature of the phases.

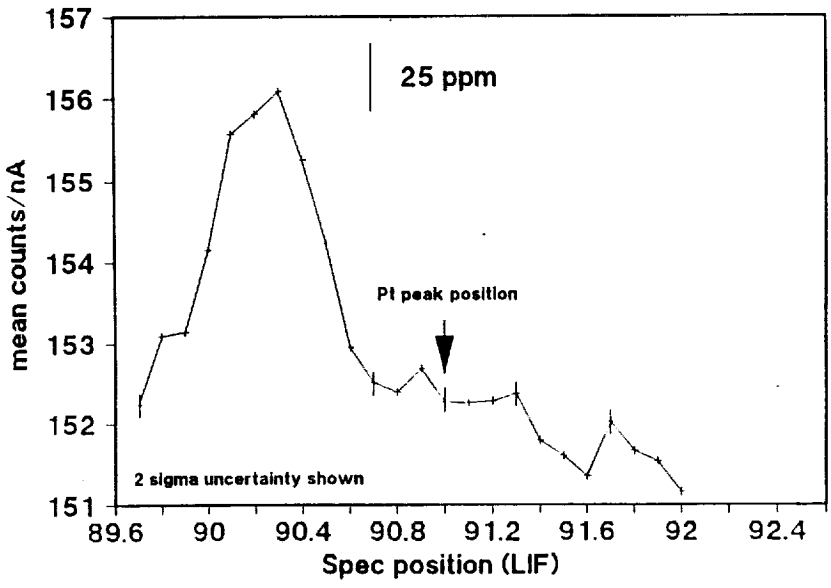

Figure 1.25 Microprobe profile across the Pt L-alpha peak illustrating the absence of Pt in the glass of experiment A12_1, suggesting significant Pt does not erode from the anodes during electrolysis. The peak observed at the left of the profile is a higher order Zn peak (although Zn was not added to these experiments, it exists as a contaminant in the reagents used to make the synthetic composition).

significant Pt is not lost from the anode. Shown as a function of oxygen generated, this is expressed as: Pt lost (mass)/oxygen produced (mass) < 1.8×10^{-3} (2 sigma uncertainty).

Papers and abstracts describing many of these results in more detail are given in the list of references. Haskin et al. (1990) is in final revision before publication, as is Haskin (1990). The papers by Colson and Haskin (1990b) and Haskin and Colson (1990) are included as Appendices D and E, respectively.

References

Colson, R. O. and Haskin, L. A., 1990a, "Lunar Oxygen and Metal for Use in Near-Earth Space: Magma Electrolysis," ASCE/AIAA Space 90 Engineering, Construction, and Operations in Space (abstract).

Colson, R. O. and Haskin, L. A., 1990b, "Lunar Oxygen and Metal for Use in Near-Earth Space: Magma Electrolysis," *Engineering, Construction, and Operations in Space* (S. W. Johnson and J. P. Wetzel, eds.) (in review).*

Haskin, L. A., 1990, "Water and Cheese From the Lunar Desert: Abundances and Accessibility of H, N, and C on the Moon," *Lunar Bases and Space Activities of the 21st Century (II)* (W. W. Mendell, ed.) (in press).

Haskin, L. A. and Colson, R. O., 1990, "Lunar Resources: Toward Living Off the Lunar Land," *Proceedings of the First Annual Invitational Symposium of the UA/NASA Space Engineering Research Center for Utilization of Local Planetary Resources* (T. Triffet, ed.) (in preparation).**

Haskin, L. A., Colson, R. O., Lindstorm, D. J., Lewis, R. H., and Semkow, K. W., 1990, "Electrolytic Smelting of Lunar Rock for Oxygen and Iron," *Lunar Bases and Space Activities of the 21st Century (II)* (W. W. Mendell, ed.) (in press).

Lindstrom, D. J. and Haskin, L. A., 1979, "Electrochemical Preparation of Useful Material From Ordinary Silicate Rocks," pages 129-134 in *Space Manufacturing Facilities* J. Grey and C. Drop, eds.), AIAA, New York.

Oppenheim, M. J., 1968, "On the Electrolysis of Molten Basalt," *Mineral. Mag.*, Vol. 36, pp. 1104-1122.

Reiger, P. H., 1987, *Electrochemistry*, Prentice-Hall, Englewood Cliffs, N.J.

Semkow, K. W. and Haskin, L. A., 1985, "Concentrations and Behavior of Oxygen and Oxide Ion in Melts of Composition $CaO{\cdot}Mg{\cdot}xSiO_2$," *Geochim. Cosmochim. Acta*, Vol. 49, pp. 1897-1908.

*See Appendix E.

**See Appendix F.